Supporting Information

High-Q and highly reproducible microdisk and microlasers

Nan Zhang [1,†], Yujie Wang [1,†], Wenzhao Sun [1], Shuai Liu [1], Can Huang [1], Xiaoshun Jiang [3,*], Min Xiao [3,*], Shumin Xiao [1,2,*], Qinghai Song [1,2,*]

1. State Key Laboratory on Tunable laser Technology, Ministry of Industry and Information Technology Key Lab of Micro-Nano Optoelectronic Information System, Shenzhen Graduate School, Harbin Institute of Technology, Shenzhen, China, 518055.

2. Collaborative Innovation Center of Extreme Optics, Shanxi University, Taiyuan 030006 China.

3. National Laboratory of Solid State Microstructures and College of Engineering and Applied Sciences, Nanjing University, Nanjing 210093, China

† These authors contribute equally to this research.

Email: # shumin.xiao@hit.edu.cn; * qinghai.song@hit.edu.cn

I. Experimental Section

1. The optical measurement setup

In the lasing experiment, the samples were mounted onto a three-dimensional translation stage under a rotating translational platform and excited by a pulsed frequency doubled Nd:YAG laser (532 nm, 7 ns, 10 Hz). The pump light was focused onto the top surface of the samples through a 10x objective lens and the beam size was adjusted to ~ 45 micron, which can well cover on the microdisk. The emitted lights were collected by a convex lens and coupled to a CCD (Princeton Instruments, PIXIS UV enhanced CCD) coupled spectrometer (Acton SpectroPro s2700) via a multimode fiber. The fluorescent microscope images were recorded by a CCD camera

behind a long pass filter. The experimental setup is shown in **Figure S1**.

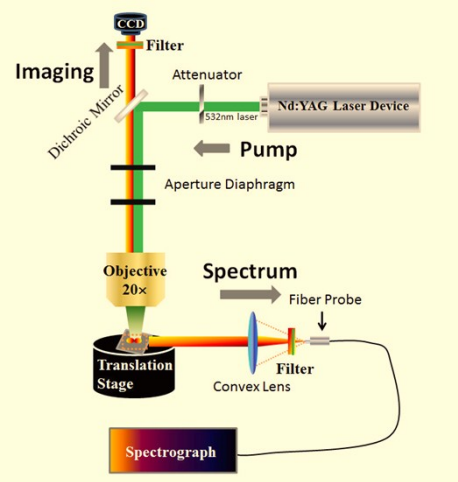

Figure S1. The setup for measuring the photoluminescence and laser emissions from the microdisk.

In the optical experiment, the tunable laser was coupled into a commercial single mode fiber. The single mode fiber was partially tapered to sub-micrometer nanofiber and pushed close to the microdisk with a three-dimensional translation stage. The transmitted laser was detected by a photodetector and recorded by a computer. The resonant modes were obtained by finely tuning the laser wavelength. When the injected laser was on resonance, it was coupled into the silicon microdisk and radiated into multiple directions. In this sense, a reduction in transmission intensity can be detected. The examples of transmitted spectra were shown in **Figure S2**.

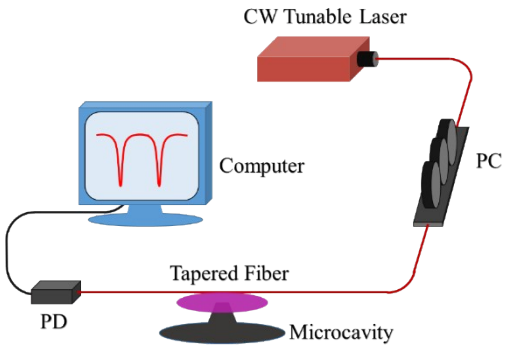

Figure S2. The setup for measuring Q factor of silicon microdisk.

2. Fabrication

The microtoroid were fabricated with a combination process of photolithography, ICP etching, wet etching and laser reflow. A commercial silicon on insulator (SOI) wafer with a 3 μm buried oxide layer and a 220 nm top silicon layer was diced into 1 cm × 1 cm chips. Next, a 2000 nm thick layer of AZ2020 negative photoresist (Microchem) was spin-coated onto the top surface and a circular array whose diameter of 100 um were patterned within the photoresist layer with a mask aligner. After developments in AZ developer, the microstructures were formed. Then an inductively coupled plasma (ICP, PlasmaPro System100 ICP) etching was applied to replicate the patterns in photoresist to the Si. During this process, the C_4F_8 with a 40 sccm flow rate was used as a protective gas. The chamber temperature was maintained at 20 degree, and the ICP and RF power was set at 1200 W and 30 W, respectively. Meanwhile, the bicomponent gas consisting of C_4F_8 and SF_6 were ionized by the ICP generator. The generated fluoride ions etched the silicon which was not protected by the AZ2020. Then the photoresist was removed and a wet etching with HF (40%) at room temperature has been utilized to transfer the pattern to SiO_2 layer. The underneath silicon was etched with the isotropic etching process of Si. During this process, we isotopically etched the silicon with SF_6 (30 W RF power, 1200 W ICP power, and chamber temperature 40 ºC). The amount etched should be approximately 1/3 of the silicon dioxide circle's size by controlling the etching time. So that the resulting microdisk's pillar is approximately 1/3-1/2 of the total disk diameter. In this way, we got the silicon dioxide microdisk. Then expose the microdisk samples to a focused CO_2 laser beam(the wavelength is 10.2 um). It is important that the center of the laser beam and the center of the microdisk are aligned, so that the silica microdisk will form a smooth, circular microtoroid.

The high Q polymer microdisk is fabricated in a dye doped SU8 film on a silicon wafer. The thickness of SU8 film is around 1.9μm and the concentration of dye is 8% in weight. Then the film baked at 170 ^{o}C for about 1 hour. The SiO_2 toroid was transferred onto the film with a tapered fiber. Using the SiO_2 toroid patterns as mask, the microdisks are fabricated by two steps of ICP etching. The first step uses O_2 to etch the dye doped SU8. The flow rate of O_2 is 10 sccm, RF power is 120 Watt, ICP power is 400 Watt, the pressure of chamber is 2 mTorr, the temperature is 20℃, and the etching time is 3 minutes. After this etching step, the SiO_2 toroid has been removed to another silicon wafer, so that it can be used later. The second step is an isotropic etching of silicon to form the pedestal underneath the microdisk. The size of pedestal is around 25 micron, which is small enough to exclude all the influences to high Q resonances.

3. The Numerical Simulation

Because the thickness of microdisk is around 5 times smaller than its in-plan size, we thus simplified the microdisks into two-dimensional objects by using the effective refractive indices n. Then, the wave equations for transverse magnetic (TM, with E perpendicular to the plane) polarized modes $E_z(x, y, z) = \psi(x, y)e^{-i\omega t}$ can be replaced by the scalar wave equation:

$$-\nabla^2\psi = n^2(x, y)\frac{\omega^2}{c^2}\psi$$

where ω is the angular frequency and c is the speed of light in vacuum.

We numerically computed the TM polarized resonances by solving the FEM with RF module in Comsol Myultiphusics 4.4. The cavity shape is defined using AutoCAD and imported into the software. A perfect matching layer is used more than 20 μm away from the boundary of limacon-spiral photonic molecule to fully absorb the outgoing waves and mimic the infinitely large space. Then complex eigenfrequencies (ω) can be obtained and then are normalized with kR = ωR/c. Here c is the speed of light in vacuum.

II. The laser action of ultrahigh-Q microdisk

1. The laser spectra in active polymer WGM microdisk

In the main text, we show the zoomed in side-view SEM images taking with 45 degree and three lasing spectra of dye-doped SU8 microdisk. The SEM image with larger magnification and the detail spectrum of active polymer microdisk with different pump energy are shown in **Figure S3**.

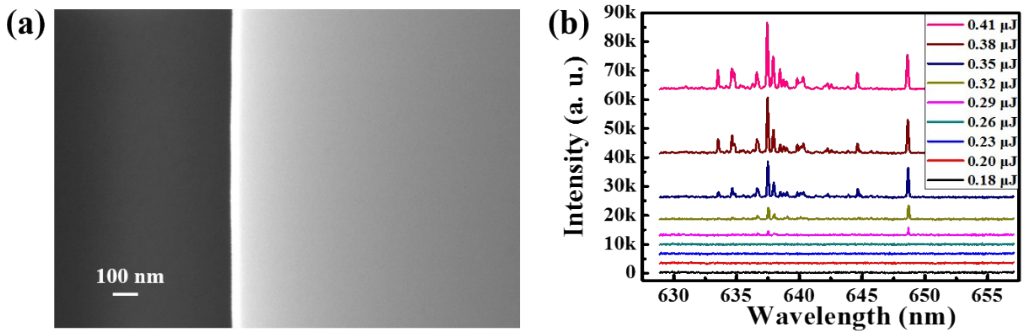

Figure S3. (a) The side-wall SEM image with larger magnification. (b) The Detail spectrum at different pump energy in active polymer microdisk.

Except the sample of active polymer microdisk that shown in the main text, we also fabricate many other samples to demonstrate the feasibility of our fabrication method. In **Figure S4**, we show the laser action of another sample.

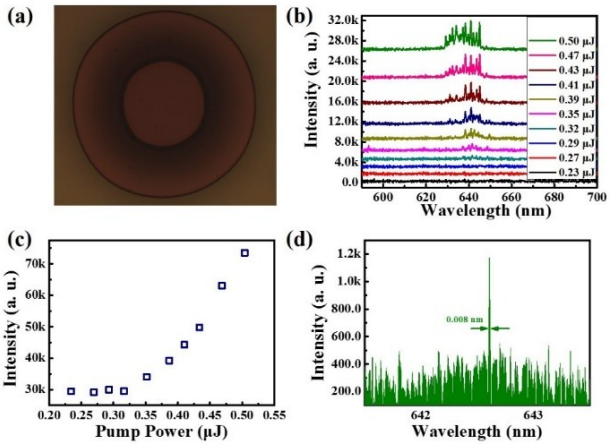

Figure S4. (a) the top-view microscope image of active polymer microdisk. (b) the detail spectrum with different pump energy. (c) the output intensity as a function of pump energy. (d) the high resolution spectrum of one laser mode. The corresponding linewidth is as small as ~ 0.008 nm.

As a contrast experiment, we have fabricated a circular microdisk with standard photolithography. In Figure S5, the relatively rough microdisk have only one to two sets of WGMs, and the corresponding linewidth is larger than 0.08 nm, which Q factor is only Q = $\lambda/\Delta\lambda = 0.8\times10^4$.

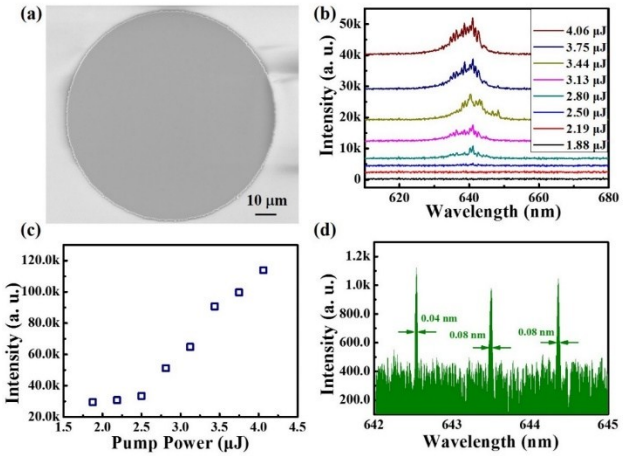

Figure S5. (a) the top-view SEM image of active circular polymer microdisk. (b) the detail spectrum with different pump energy. (c) the output intensity as a function of pump energy. (d) the high resolution spectrum of one laser mode. The corresponding

linewidth is ~ 0.08 nm.

In the main text, we mentioned the reproducibility of polymeric microdisk. Here we show the detailed laser action of the four disks. In **Figure S6-S9**, we can see that the resonant frequencies, linewidths, peak numbers, and laser threshold are all the same in four microdisks. Therefore, we know that replicating high-Q microtoroid in polymer with ICP etching can simply solve the challenge in reproducibility and have great potentials in fabricating highly reproducible microdisks.

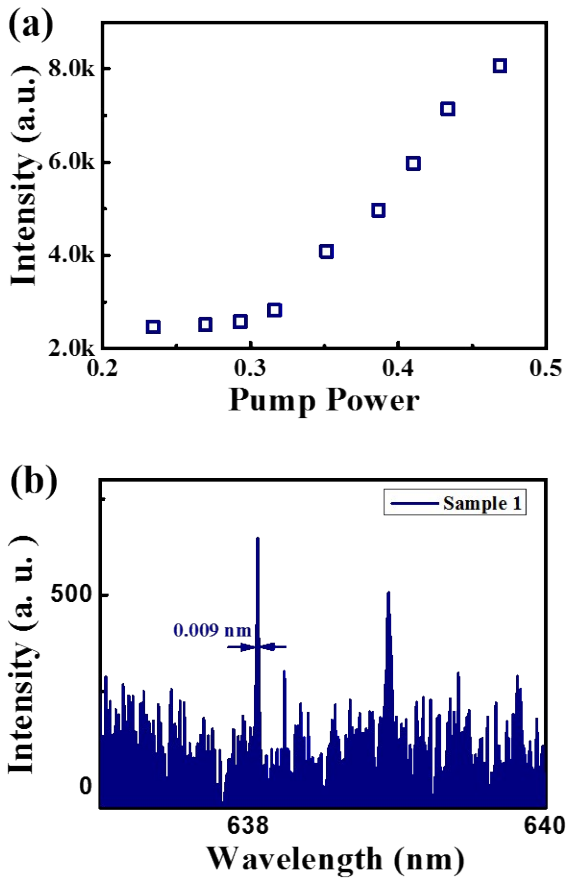

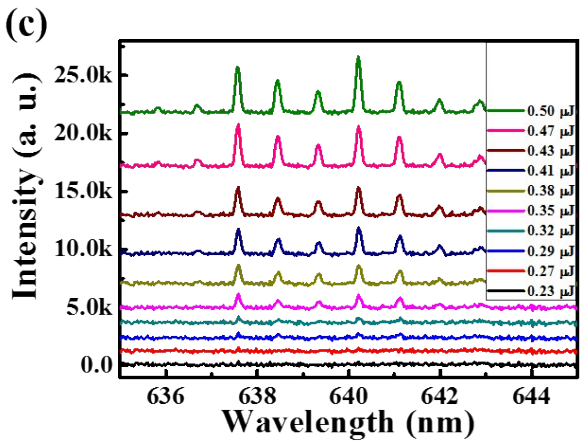

Figure S6. The laser action of disk-1. (a) the output intensity as a function of pump energy. (b) the high resolution spectrum of one laser mode. The corresponding linewidth is ~ 0.09 nm. (c) the detail spectrum with different pump energy.

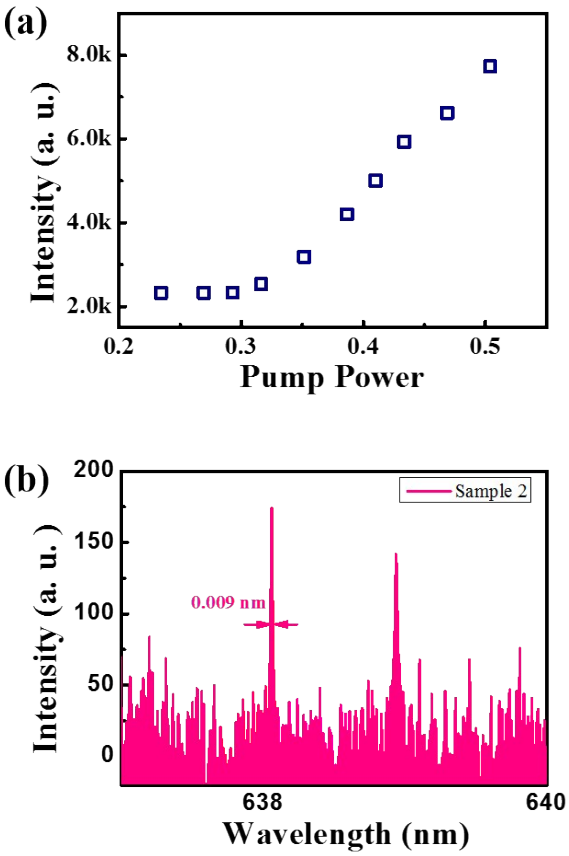

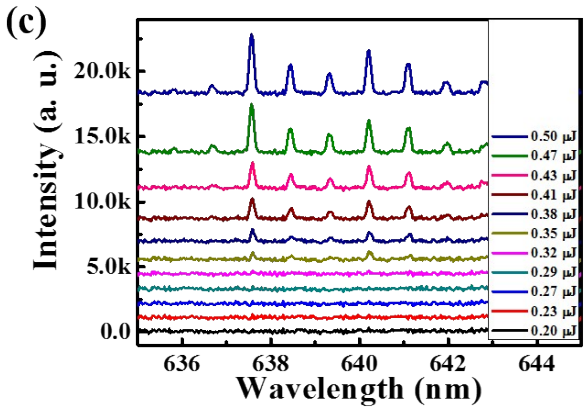

Figure S7. The laser action of disk-2. (a) the output intensity as a function of pump energy. (b) the high resolution spectrum of one laser mode. The corresponding linewidth is ~ 0.09 nm. (c) the detail spectrum with different pump energy.

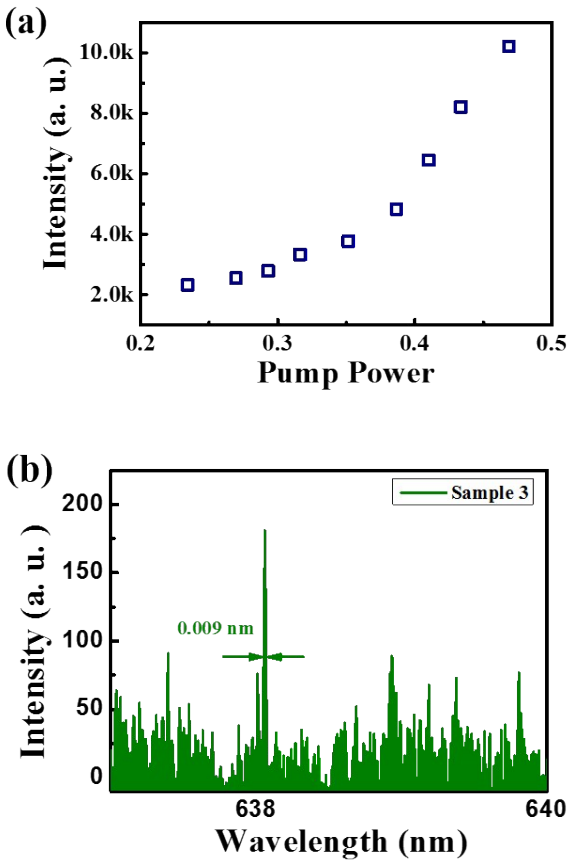

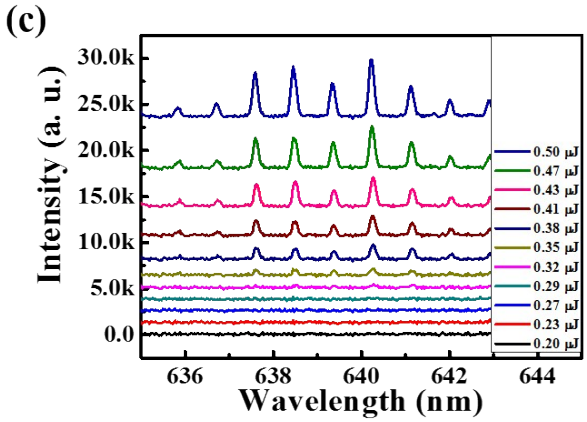

Figure S8.The laser action of disk-3. (a) the output intensity as a function of pump energy. (b) the high resolution spectrum of one laser mode. The corresponding linewidth is ~ 0.09 nm. (c) the detail spectrum with different pump energy.

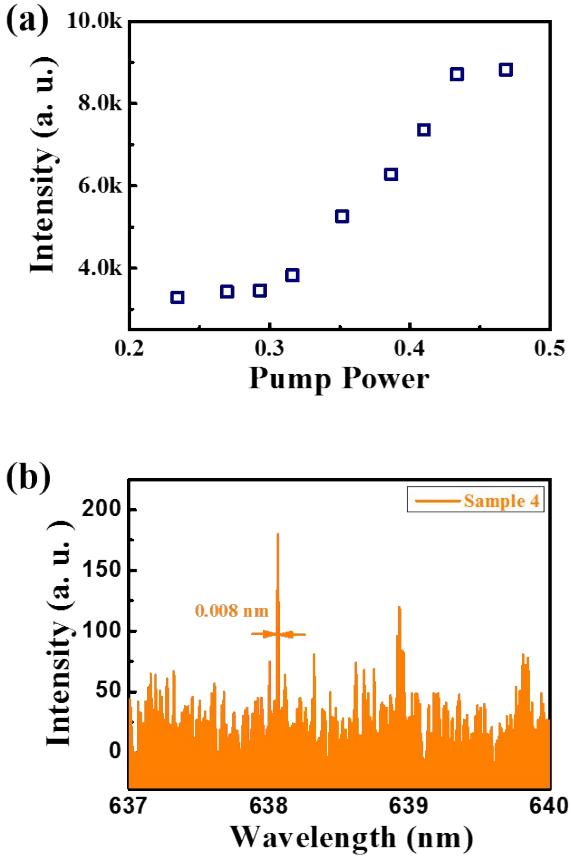

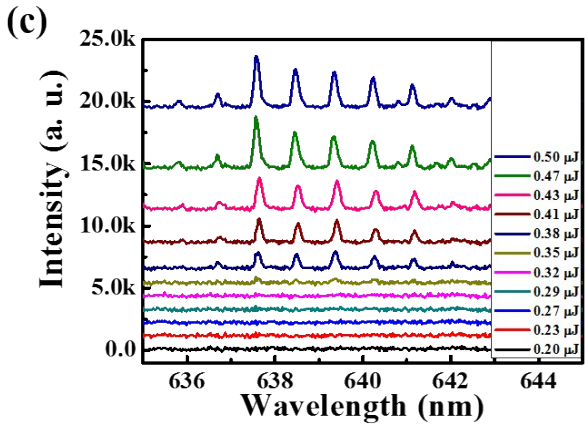

Figure S9. The laser action of disk-4. (a) the output intensity as a function of pump energy. (b) the high resolution spectrum of one laser mode. The corresponding linewidth is ~ 0.08 nm. (c) the detail spectrum with different pump energy

2. The tansmission spectra in passive polymer microdisk

In the main text, we measured the Q factor of the polymer microdisk. And we obtain the example of transmitted spectra. The detail spectrum of polymer microdisk is shown in **Figure S10**.

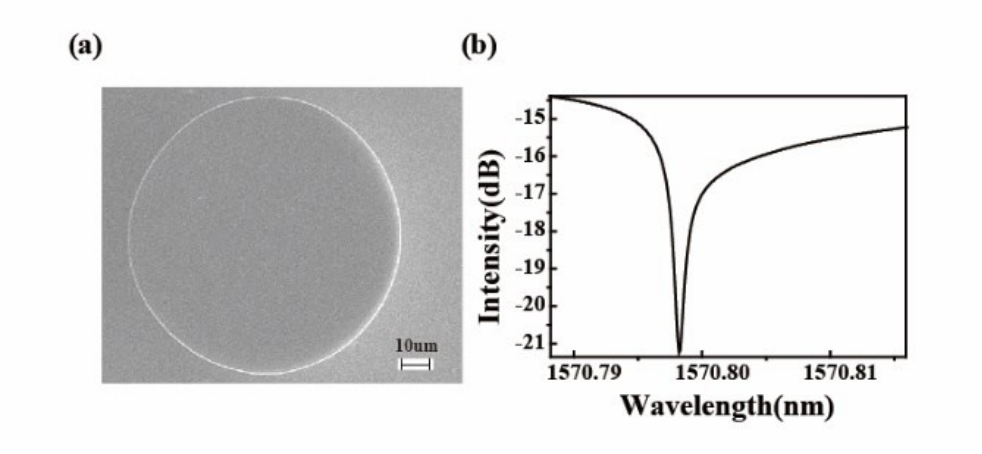

Figure S10. (a) is the SEM images of polymer microdisk. (b) is the experimentally recorded transmission spectra of polymer microdisk.

3. The FSR in microdisk

Free spectral range (FSR) is one of the key specifications of the ring resonator.

In the main text, we measured the Q factor of the polymer microdisk and the silicon microdisk and obtain the example of transmitted spectras. Through the calculation, the value of the FSR matched the data we measured. The detail spectrum of polymer and silicon microdisks are shown in **Figure S11** and **Figure S12**.

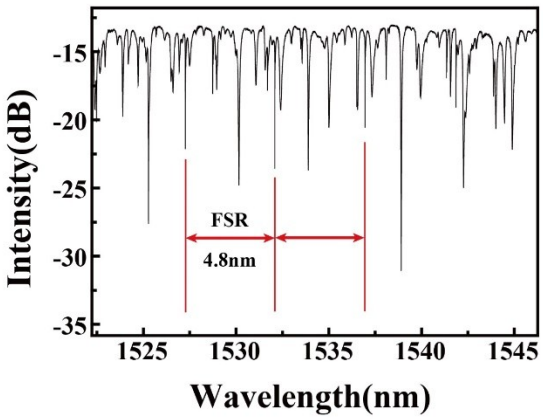

Figure S11. The transmission spectrum in passive polymer microdisk, here the FSR is 4.8nm.

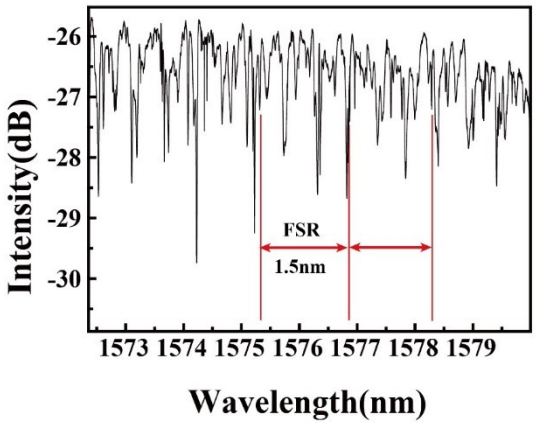

Figure S12. The transmission spectrum in silicon microdisk. Here the FSR is 1.5nm.

4. The laser spectra in active polymer limacon microdisk.

In lasing experiment of limacon microdisk, due to the presents of mirror-reflection symmetry, the CW and CCW components are balanced and two directional

emissions along φFF= ±60° can be formed in far field which is well matched with the numerical results. When we pumped the microdisk, there are two dominated modes. The far field angular distribution of the total emission has been shown in Figure 4. In **Figure S13** we shown the detail experiment results.

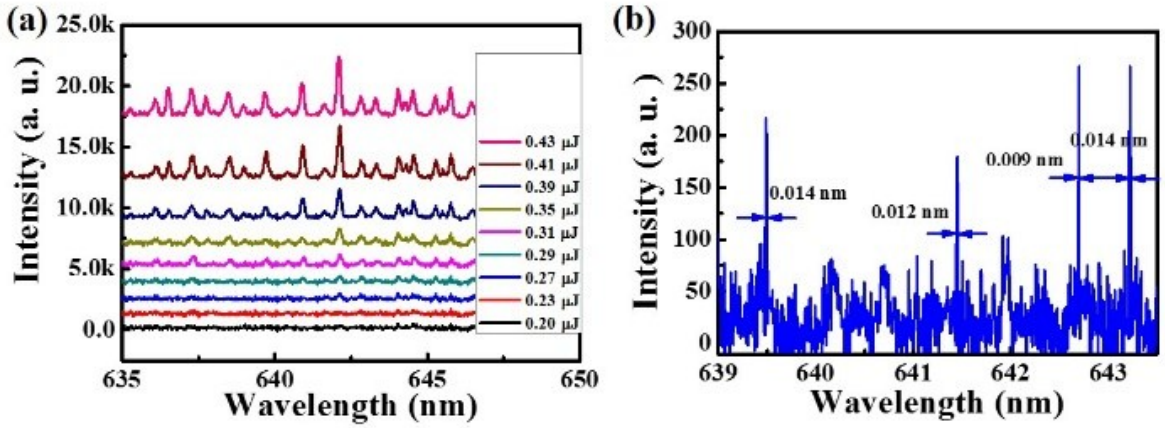

Figure S13. (a) the detail spectrum with different pump energy. (b) the high resolution spectrum of one laser mode. The corresponding linewidth is ~ 0.09 nm.

Besides the observation of laser actions in the limacon microdisk, it is more important and essential to detect far field pattern. We then rotated the translation stage and recorded the laser spectrum at every 5 degree. In Figure 4, we shows the angular distribution of the emissions at far field pattern. Here we shown the detail spectrum with different angles (see **Figure S14**).

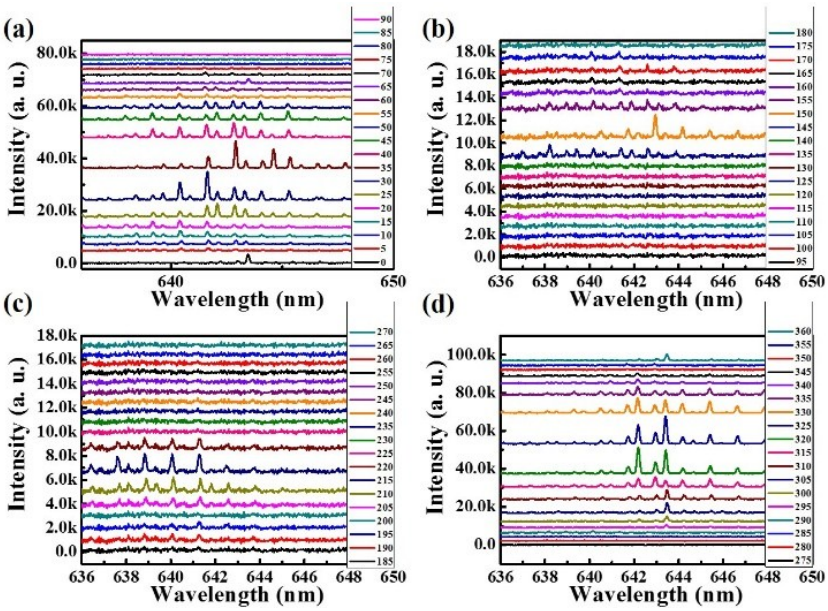

Figure S14. (a), (b), (c) and (d) are the detail spectrum of limacon at different collection angles.

In this main text, we have mentioned the field pattern in Figure 4. Here we show logscale polt in **Figure S15**. Different from the figures in the main text, here the emissions from the cavities can be clearly seen. In the limacon microdisk, two directional laser beams can be seen. Therefore, we can confirm that high-Q microdisks lasers can also be replicated from microtoroids via anisotropic ICP etching.

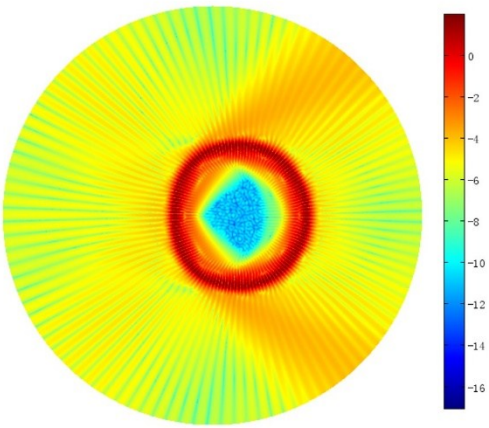

Figure S15. The logscale plot of field patterns, this correspond to the field patterns in Figure 4(d) in the main text.

III. Ray dynamics of limacon cavity in Poincare surface of section (PSOS)

The ray dynamics of limacon cavity has been thoroughly studied in literatures. Here we show the details of our cavity. As shown in Figure S16, the PSOS is dominated by the chaotic motions. Here the x-axis and y-axis correspond to the point that a ray hits the cavity boundary (ϕ) and the incident angle (χ). While stable islands do exist, they are far below the critical line (the red dashed line in **Figure S16**). Meanwhile, there are some whispering-gallery like modes at very large $\sin\chi$ (> 0.99). For the generality, we consider the chaotic modes that are localized along unstable periodic orbits in chaotic sea via wave localization (see the calculated modes in the main text).

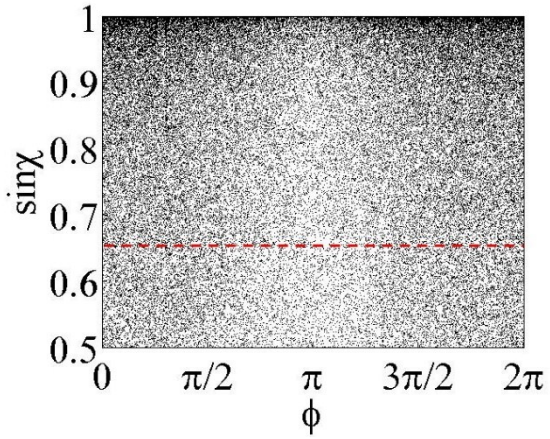

Figure S16. The ray dynamics of limacon cavity with $\varepsilon = 0.45$ in Poincare surface of section.